Evolution of Raman G and G' ($2D$) modes in folded graphene layers

Chunxiao Cong[1] and Ting Yu[1,2,3,*]

[1]*Division of Physics and Applied Physics, School of Physical and Mathematical Sciences, Nanyang Technological University, 637371, Singapore*

[2]*Department of Physics, Faculty of Science, National University of Singapore, 117542, Singapore*

[3]*Graphene Research Center, National University of Singapore, 117546, Singapore*

(Received 6 March 2014; revised manuscript received 22 May 2014; published 23 June 2014)

Bernal- and non-Bernal-stacked graphene layers have been systematically studied by Raman imaging and spectroscopy. Two dominant Raman modes, G and G' (or $2D$), of folded graphene layers exhibit three types of spectral features when interlayer lattice mismatches, defined by a rotational angle varies. Among these folded graphene layers, the most interesting one is the folded graphene layers that present an extremely strong G mode enhanced by a twist-induced Van Hove singularity. The evolution of Raman G and G' modes of such folded graphene layers are probed by changing the excitation photon energies. In this paper, doublet splitting of the G' mode in a folded double-layer ($1 + 1$) and of the G mode in a folded tetralayer ($2 + 2$) graphene are observed and discussed. The G' mode splitting in folded double-layer graphene is attributed to the coexistence of inner and outer scattering processes and the trigonal warping effect as well as further downward bending of the inner dispersion branch at a visible excitation energy. The two peaks of the G mode in folded tetralayer graphene are assigned to Raman-active mode (E_{2g}) and lattice mismatch activated infrared-active mode (E_{1u}), which is further verified by the temperature-dependent Raman measurements. Our study provides a summary and discussion of Raman spectra of Bernal- and non-Bernal-stacked graphene layers and further demonstrates the versatility of Raman spectroscopy for exploiting electronic band structures of graphene layers.

DOI: 10.1103/PhysRevB.89.235430 PACS number(s): 78.30.Na, 81.05.ue, 63.20.kd, 78.67.Pt

I. INTRODUCTION

Electronic band structures of graphene layers are remarkably influenced by the ways these carbon atomic layers stack themselves. The most stable and common one is AB (or Bernal) stacking. From pristine monolayer to Bernal-stacked bilayer and few-layer graphene, electronic band structures show significant differences and can be effectively probed by investigating their Raman spectral features such as relative intensities, linewidths, line shapes, and peak positions of Raman G and G' (or $2D$) modes through the strong electron-phonon coupling [1–6]. Such unique optical responses promise that Raman spectroscopy will be a widely adapted technique to quickly and precisely identify thicknesses of pristine Bernal-stacked graphene layers. However, when such graphene layers are subjected to some local electrical or mechanical perturbations, for example, varying local electrical potential by coating molecules or applying electrical gate [7–13] or expanding the substrate where graphene layers anchor by applying uniaxial strain [14–17], Raman modes of G and G' could change remarkably. Thus, one should pay special attention to determine the number of layers of graphene by using the spectral features of Raman G and G' modes. In addition to the perfect Bernal stacking, graphene layers may naturally or artificially stack themselves into other sequences, which also lead to the different Raman spectral features compared to Bernal-stacked ones. The two most well-known non-Bernal-stacked graphene layers are ABC-stacked trilayer graphene and $1 + 1$ folded or twisted double-layer graphene (fDLG or tDLG). As being widely used in the studies of graphite and carbon nanotubes [18,19], Raman spectroscopy once again has demonstrated its special and powerful ability to probe the electronic band structures of two such interesting two-dimensional carbon systems. Quick and accurate identification and even visualization of ABC-stacked trilayer graphene domains from Bernal-stacked ones by Raman imaging and spectroscopy have been successfully demonstrated [20,21]. Modulation of electronic band structures by a stacking defect such as a twist was predicted by the theoretical study at the early stage of graphene investigation [22], and the proposed remaining of linear dispersion and reduction of Fermi velocity were evidenced by the Raman spectroscopy study of the G' mode in a $1 + 1$ fDLG soon afterward [23]. Later, an extremely strong G mode, i.e. tens of times stronger than the G' mode, was observed in the fDLG [24]. On the contrary, of the well-known dispersive D mode, a nondispersive defect (rotational stacking) mode was seen and explained as the rotational angle dependent wave vector assisted double resonant scattering process [25]. To prepare fDLG with more folding or rotational angles, a flipping over technique was developed by using an atomic force microscope (AFM) [26,27]. New peaks, next to the G mode at both lower and higher frequency regions, appeared in such fDLG, which are also activated by the period static potential defined by the rotational angles or the wave vector in the superlattice [26,27]. Large-scale growth of graphene layers by chemical vapor deposition (CVD) offers feasibility of producing tDLG with a wide range of twisting angles by transferring one layer followed by the other or locating the as-grown tDLG with multiple domains [28–30]. More direct evidence of the change of electronic band structure by rotational stacking such as the twist-induced Van Hove singularities (VHS) was given by a scanning tunneling microscopy/spectroscopy study of

*Corresponding author: yuting@ntu.edu.sg

twisted CVD graphene double layers [31]. From transmission electron microscopy (TEM) diffraction patterns, orientations of domains and consequently twisting angles between two graphene layers can be precisely determined. Combining TEM and Raman spectroscopy, the Raman G and G' modes of tDLG with twisting angels from 0 to 30° were systematically studied [28,30]. The twist-induced VHS could be clearly reflected by the dramatic enhancement of the Raman G mode [30]. Meanwhile, the spectral features such as linewidths, frequencies, and intensities also show dependence on the twisting angles, demonstrating that the Raman G and G' modes can be used to identify the twisting angles [28,30]. Most recently, CVD-grown tDLG consisting of a single domain in each layer was studied by Raman spectroscopy [32,33]. Twist-induced Raman modes of low and intermediate vibrational frequencies were also observed [29,32,33].

In this paper, we focus on the dominant Raman G and G' modes and exploit their evolution in graphene layers of different stacking orders, including both Bernal and non-Bernal ones. In addition to $1 + 1$ fDLG, we also studied $2 + 2$ folded tetralayer graphene (f4LG). Here, the 2 refers to Bernal-stacked bilayer graphene (BLG). Such $2 + 2$ f4LG are hardly prepared by CVD and are rarely studied. By carefully checking the spectral features such as relative intensities, line shapes, linewidths, and peak positions, three patterns of Raman G and G' modes are identified, corresponding to the graphene layers of three types of rotational stacking defined by three ranges of rotational angles, θ. In detail, for the excitation photon energy of 2.33 eV, the first group has a relatively small rotational angle below 4° (named as θ_{small}), the second group possesses a rotation angle of around 11° (named as θ_{medium}), and rotational angles are more than 20° for the third group (named as θ_{large}). Among these different types of folded graphene layers, the most interesting one shows strong enhancement of the G mode intensity due to the twist-induced VHS (our labeling, θ_{medium}). Doublet splitting of the G' mode for $1 + 1$ fDLG θ_{medium} samples and of the G mode for $2 + 2$ f4LG θ_{medium} samples are noticed through the investigation of the evolution of these two modes under different excitation photon energies. Our further polarization- and temperature-dependent Raman spectroscopy studies reveal that the splitting is due to the coexistence of inner and outer scattering processes and the trigonal warping effect for the G' mode and Raman-active mode (E_{2g}) and stacking defect-activated infrared (IR)-active mode (E_{1u}) for the G mode.

II. EXPERIMENT

All graphene layers in this paper were prepared by the mechanical cleavage of graphite and transferred onto a 300-nm SiO_2/Si substrate. The folded graphene layers were self-formed by accident during the mechanical exfoliation process. An optical microscope was used to locate the folded thin layers, and the number of layers of the unfolded part was further identified by white light contrast spectra and Raman spectroscopy [34]. The Raman images were acquired using a WITec CRM200 Raman system with a 600 lines/mm grating and a piezocrystal controlled scanning stage under 532 nm ($E_{\text{laser}} = 2.33$ eV) laser excitation. A grating of 2400 lines/mm was used for single Raman spectrum measurements under different excitation energies to achieve high spectral resolution. For the room temperature Raman measurements, an objective lens of 100× magnification and 0.95 numerical aperture (NA) was used, and the laser spot was ~500 nm in diameter. The laser power was kept below 0.1 mW on the sample surface to avoid laser-induced heating. For the temperature-dependent Raman measurement, a long-working-distance 50× objective with NA of 0.55 was used, and the sample temperature was controlled by a programmable hot stage HFS600E from Linkam Scientific Instruments.

III. EXPERIMENTAL RESULTS AND DISCUSSION

Though the variation of the general Raman spectral features of the G and G' modes were observed and discussed in tDLG grown by CVD over a wide range of rotational angles, more details need to be investigated [30,35]. Figure 1 presents the Raman images and spectra of three types of fDLG and pristine single-layer graphene (SLG) obtained under the excitation photon energy of 2.33 eV together with the optical image and the schematic illustration. In this paper, unless specially clarified, all Raman images were plotted by extracting the spectral features through a single Lorentzian line shape fitting. The folding angles were measured from both the optical and AFM images, as previously reported [24] (see Supplemental Material and Fig. S1 for more details [36]), and are shown next to the corresponding Raman spectra [see Fig. 1(c)]. Compared to the SLG, all G' modes of fDLG show a blueshift due to the reduction of Fermi velocity [22,23]. For the sample shown in panel (a) and labeled as θ_{small}, the Raman D mode image [Fig. 1(a5)] further indicates the dominant edge orientations, as also illustrated schematically by light blue honeycomb in Fig. 1(a5) [37–39]. As shown, for the fDLG of a small twisting angle (less than 4°), our θ_{small}, integrated intensity of the G' mode, is even weaker than that of SLG [Fig. 1(a6)], whereas the linewidth is much larger than that of SLG [Fig. 1(a8)]. The corresponding Raman spectrum [Fig. 1(c)] of the $1 + 1$ fDLG θ_{small} sample displays a broad asymmetric G' peak consisting of multiple subpeaks instead of a narrow single symmetric peak appearing in the spectrum of SLG. This might be due to the formation of a Bernal-stacked BLG-like electronic structure led by the strong interlayer interaction and highly overlapping of two cones of each layer [40]. More details of the asymmetric Raman G' mode of $1 + 1$ θ_{small} fDLG under different excitation energies are shown in the support information together with that of Bernal-stacked BLG (see Supplemental Material Fig. S2 [36]). It shows that the broad and asymmetric Raman G' mode of $1 + 1$ θ_{small} fDLG can be fitted well by four Lorentzian peaks, which are usually used for fitting of the Raman G' mode of AB-stacked BLG. The frequencies of all of the four subpeaks of $1 + 1$ θ_{small} fDLG increase linearly with an increase of the excitation energy, which is similar to that of AB-stacked BLG. This, in some ways, indicates the similarity of the electronic structures between the $1 + 1$ θ_{small} fDLG and the AB-stacked BLG. The sample shown in panel Fig. 1(b) contains two folded areas, as also illustrated in Fig. 1(b5). The most obvious difference between the Raman spectral features of these two fDLG is the remarkable contrast of G mode intensities [Fig. 1(b2)] or the relative intensities between the G and G' mode [Fig. 1(c)]. The

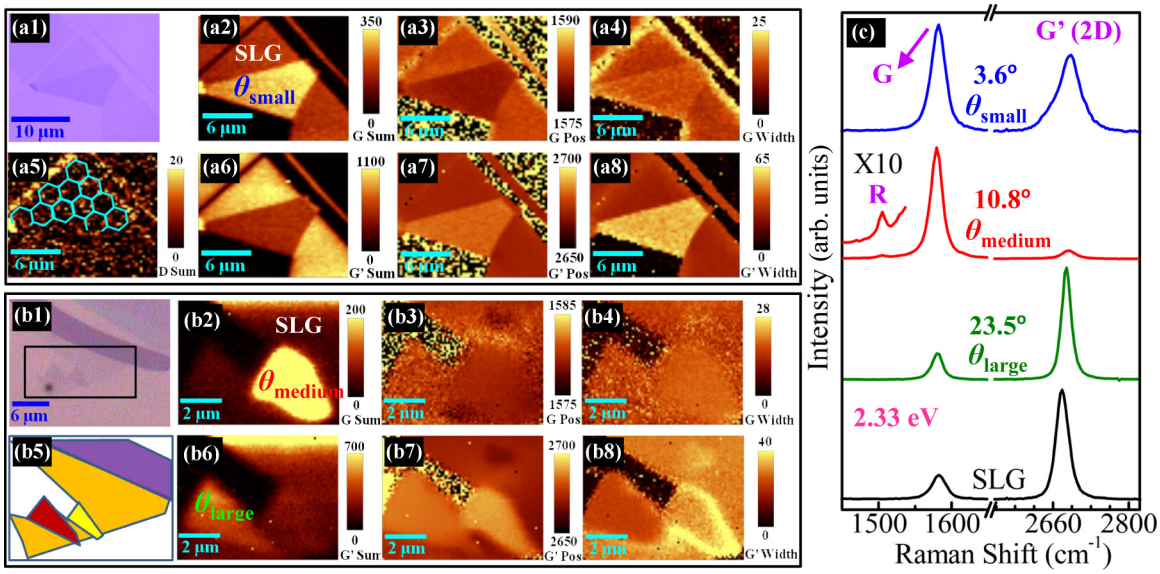

FIG. 1. (Color online) Panels (a1) and (b1) show the optical images of different folded double-layer graphene sheets. Panels a2 (a6), a3 (a7), and a4 (a8) are Raman images of the G (G') mode integrated intensity, the G (G') mode frequency, and the G (G') mode width of the corresponding folded double-layer graphene samples shown in panel (a1). Panels b2 (b6), b3 (b7), and b4 (b8) are Raman images of the G (G') mode intensity, the G (G') mode frequency, and the G (G') mode width of the corresponding folded double-layer graphene samples shown in panel (b1). (a5) is the Raman image of the D mode intensity of the edges of the single-layer sheet shown in (a1), which indicates the crystal orientation (illustrated by the light blue honeycomb) of the single-layer sheet and the twisting angle of the folded double-layer graphene. (b5) is the schematic image of the two folded double-layer parts shown in (b1). (c) The Raman spectra of the corresponding folded double-layer graphene sheets and together with the single-layer graphene shown in (a1) and (b1). The excitation energy is $E_{\text{laser}} = 2.33$ eV.

significant enhancement of the G mode in our $1 + 1$ fDLG θ_{medium} sample can be well interpreted by the resonant effect between the conduction and valence twist-induced VHS [30]. A small R peak can be also seen in this fDLG θ_{medium} sample, which is activated and defined by the twist-induced wave vector in the superlattice [26]. Very practically meaningful, this R peak could be a good indicator of rotational angles, as demonstrated previously [27,29]. The interlayer coupling in our fDLG θ_{large} samples is relative weak. The G' mode remains the same line shape as that of SLG and is much stronger than the G mode. It should be noticed that the types of our clarifications and Raman spectral patterns are both rotational-angle- and excitation-photon-energies-dependent. For different laser lines, the same folded type may appear at different rotational angles.

To further exploit the Raman G and G' modes of these three types of fDLG, the evolutions of these two modes under different excitation energies are studied. Figure 2 shows the laser-excitation-energy-dependent Raman spectra of fDLG together with that of SLG as a comparison. Owing to the dispersive nature and the double resonant scattering process, all G' modes show blueshift as the increase of the excitation photon energies while the zone center G phonons keep a constant vibrational frequency. Our focus of this part is the θ_{medium} sample as it demonstrates the most remarkable change [Fig. 2(c)]. First, the small R peak does not shift when changing the excitation energies. As reported, this is because that the R peak is mediated by the twist-induced wave vector, which is strictly defined by the rotational angles [26]. Therefore, once the rotational angle is fixed, the wave vector is defined, and then the momentum and subsequently the energy of phonons are fixed or selected, leading to the nondispersion of the R peak [26]. Using this criterion and the plots in Ref. [26], the position of 1506 cm^{-1} corresponds to a rotational angle of 11°, which is very close to our measured value of 10.8°. Very different from θ_{small} (BLG-like) or θ_{large} (SLG-like), the G' mode of θ_{medium} fDLG samples present a very obvious doublet splitting under a higher excitation energy, 2.54 eV in this paper. The doublet splitting of G' mode has been observed in suspended [41,42] or uniaxially stretched SLG [43–45]. In the latter case, the G' peaks would show substantial redshift and broadening [15–17], which are absent in our data. Therefore, we would temporarily consider our observations along the track of the arguments on bimodal G' mode line shape in suspended SLG. By suspending the SLG and consequently suppressing the substrate induced unintentional doping, the doping induced broadening effects on Raman G' modes could be weakened, and the intrinsic narrow subpeaks will be resolved if there are any [41,42]. If the excitation photon energy is high enough to pump electrons to a level where the Dirac cone is distorted and a triangular-shaped equal energy contour is present, the so-called electronic trigonal warping effect together with the phononic trigonal warping effect will play critical roles in the electron-phonon double resonant scattering process and could be responsible for the G' mode splitting [41,42,46].

To further understand this doublet splitting of the G' mode in the fDLG θ_{medium} sample, we performed careful curve fitting of the spectra under different excitation energies and polarization-dependent Raman spectroscopy measurements. From the electronic band structure of pristine SLG, the trigonal warping effect becomes more obvious at a relatively higher energy level, and even the electronic dispersions are no longer

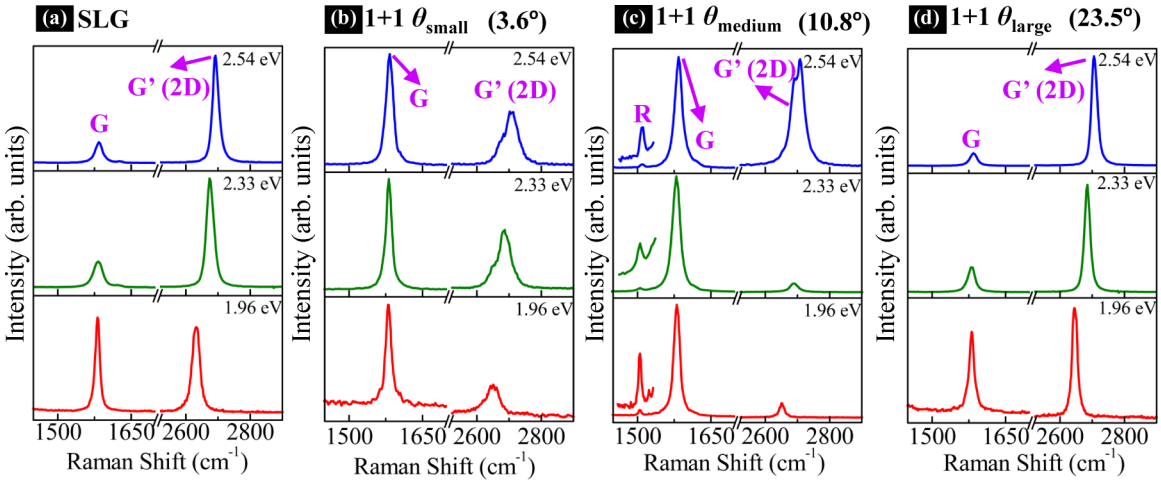

FIG. 2. (Color online) Laser-excitation energy-dependent Raman spectra of (a) single-layer graphene, (b) folded double-layer graphene of θ_{small}, (c) folded double-layer graphene of θ_{medium}, and (d) folded double-layer graphene of θ_{large}.

perfectly linear, for example, bending towards lower energy level along the *K*-*M* direction, which corresponds to the inner scattering process, whereas the dispersion along the *K*-Γ direction for the outer scattering process bends upward [46]. Such evolution of electronic band structure at a relatively high energy level should immediately cause the higher frequency G' peak ($G'+$) to move further away from the lower frequency one ($G'-$) [41,46]. It should be noticed that the phonon trigonal warping effect could also affect the positions of two G' peaks from the inner and outer scattering processes. An earlier study [46] has clearly demonstrated that the separation of these two peaks still increases when the excitation energy is beyond 2.3 eV by considering both phononic and electronic trigonal warping effects [46]. Our previous experimental study Luo *et al.* [41] on the suspended SLG clearly showed that the separation of the two G' peaks increases from 12 cm^{-1} in the visible excitation photon energy to ~20 cm^{-1} under ultraviolet light of 3.49 eV. As shown in Fig. 3(a), with the increase of the excitation energies, the Raman frequency separation between the $G'+$ mode and the $G'-$ mode of θ_{medium} fDLG indeed increases. This agrees well with the theoretical predication of SLG at higher excitation energies [41,46]. Slightly different from the previous studies [41,42], the increment of the frequency difference in the visible excitation photon energy range for our θ_{medium} fDLG sample could possibly result from the further downward bending of the dispersion along the *K*-*M* direction induced by the twist even in the visible excitation photon energy range besides the phononic and electronic trigonal warping effects [40]. Therefore, we tentatively assign the higher frequency component ($G'+$) to the inner scattering process and the lower frequency component ($G'-$) to the outer scattering process. The relative intensity of the $G'+$ feature (inner process) over the $G'-$ feature (outer process) is considerably complicated in the folded or twisted graphene layers because there is an anisotropic contribution to the G' mode in the phonon Brillouin zone and such nonuniformity varies when the rotational angles change [35]. This aspect is out of the scope of this paper. The schematic diagrams of the inner and outer scattering processes of the G' mode in pristine SLG and our θ_{medium} fDLG are shown in Supplemental Material Fig. S3 [36]. Another consequence of the trigonal warping effects, also being an effective way to probe such an effect, is the different response of $G'-$ and $G'+$ modes to the

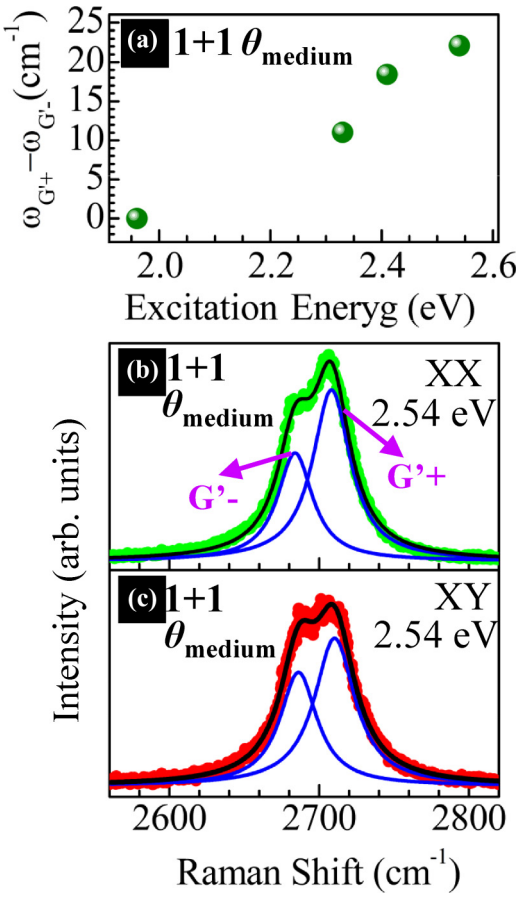

FIG. 3. (Color online) (a) Frequency separation of the $G'+$ mode and $G'-$ mode as a function of the laser-excitation energy. Here, we fitted the G' mode of the $1+1$ θ_{medium} sample by two Lorentzian peaks. (b), (c) Raman spectra of G' mode with fitted curves of folded double-layer graphene of θ_{medium} done with different light polarization under the excitation energy of 2.54 eV.

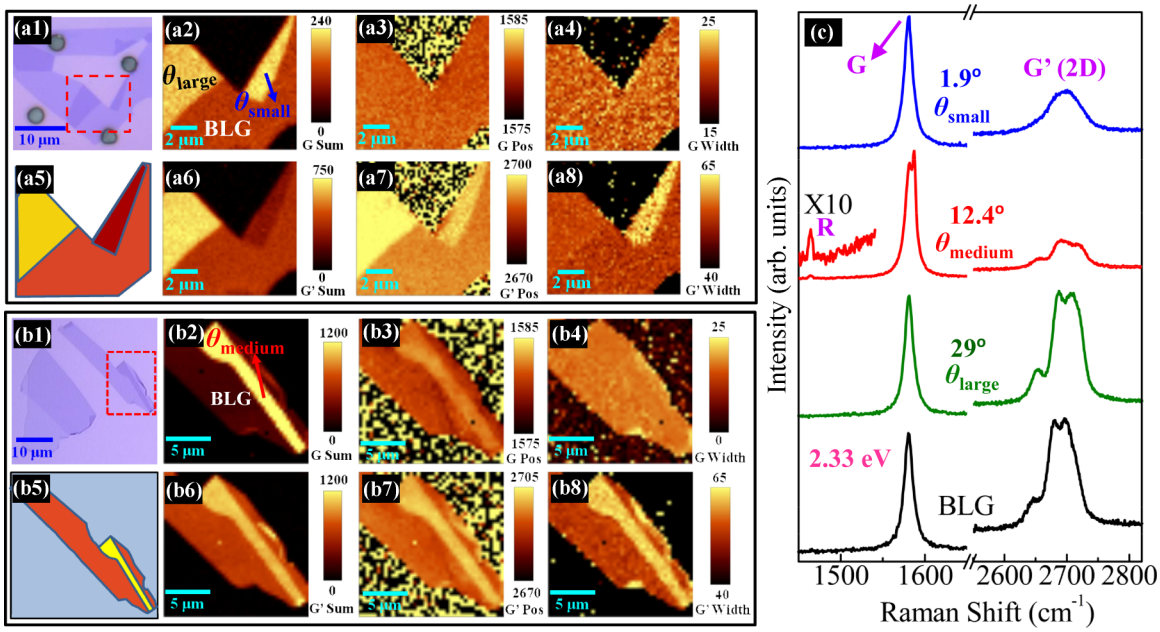

FIG. 4. (Color online) Panels a1 (a5) and b1 (b5) show the optical images (schematic images) of different folded tetralayer graphene samples. Panels a2 (a6), a3 (a7), and a4 (a8) are Raman images of the G (G') mode integrated intensity, the G (G') mode frequency, and the G (G') mode width of the corresponding folded tetralayer graphene samples shown in panel (a1). Panels b2 (b6), b3 (b7), and b4 (b8) are Raman images of the G (G') mode integrated intensity, the G (G') mode frequency, and the G (G') mode width of the corresponding folded tetralayer graphene samples shown in panel (b1). (c) The Raman spectra of the corresponding folded tetralayer graphene sheets and together with the AB-stacked bilayer graphene shown in (a1) and (b1). The excitation energy is $E_{\text{laser}} = 2.33$ eV.

polarization configuration of the incident and scattering lights. Due to the triangular shape or the different curvatures of the electronic band structures facing the K-M (inner scattering) and K-Γ (outer scattering) directions, the anisotropic optical absorption around the K point [47], and also the dependence of Raman G' intensity on involved phonon wave vector directions [46], the relative intensity of outer scattering process over inner scattering process could be very different at different polarization conditions. As shown in Figs. 3(b) and (c), under the parallel polarization (XX), the $G'+$ is more dominant, which perfectly agrees with the previous findings of Raman G' band of SLG at higher excitation energies [46]. Considering the above discussion about the dependence of the G' mode of the θ_{medium} fDLG on the excitation energy and polarization, we tentatively attribute the doublet splitting of the G' band here to the coexistence of the inner and the outer scattering processes and the trigonal warping effects as well as further downward bending of the inner dispersion branch at visible excitation energy [40]. The arguments of outer and inner scattering processes in the G' phonons have been a long-lived debate. Our findings demonstrate that the folded or twisted graphene layers could be an interesting system for such topic. More systematic study is needed.

Though $1 + 1$ fDLG (or tDLG) has been intensively studied, $2 + 2$ f4LG is rarely investigated. As shown in Fig. 4, very similar to the fDLG, $2 + 2$ f4LG also exhibits three types. For the $2 + 2$ θ_{medium} f4LG, the G mode also shows an enhancement compared to that of AB-stacked BLG under the excitation energy of 2.33 eV, as can be seen from the Raman image of Fig. 4(b2) and the Raman spectra of Fig. 4(c). The enhancement of the G band in $2+2$ θ_{medium} f4LG should share the same mechanism of that in $1 + 1$ θ_{medium} fDLG, which is due to the resonance of the energy between the conduction and valence VHS with the excitation photon energy [30]. Our simulation clearly reveals the formation of VHS in $2 + 2$ θ_{medium} f4LG, and the energy between the conduction and valence VHS has a good correspondence with our excitation photon energy [48]. Different from the fDLG, the G mode of θ_{medium} f4LG shows a doublet splitting, and two subpeaks are clearly resolved [Fig. 4(c)]. It is known that G-mode splitting or two-peak G mode occurs when the graphene layers are highly and asymmetrically doped at top and bottom layers, which causes the breaking inverse symmetry and consequently the phonon mixing [49–52]. Applying a substantially large uniaxial strain could also split the G mode by breaking the symmetry of the lattice and subsequently breaking the degeneracy of the twofold symmetric E_{2g} phonons [15,16,49]. However, for this paper, neither of the above two circumstances apply since we did not highly dope or substantially stretch the samples, as evidenced by the absence of a large amount of blueshift, the response of doping [12] and the lack of redshift of the G mode, the response of tensile strain [14,17]. Two Raman modes, D' and R', are also located near the G mode and at the high frequency side. However, the truth that both two peaks are much weaker than that of G peak [26,29] unambiguously indicates that neither of them could be responsible for the observed very sharp and strong $G+$ mode here.

To further unveil the origin of the doublet splitting of the G mode in our θ_{medium} f4LG, first we conducted excitation-energy-dependent Raman measurements and plotted the Raman spectra in Figs. 5(a)–(c). It is clear enough that the second G peak ($G+$) appears when the normal G mode ($G-$)

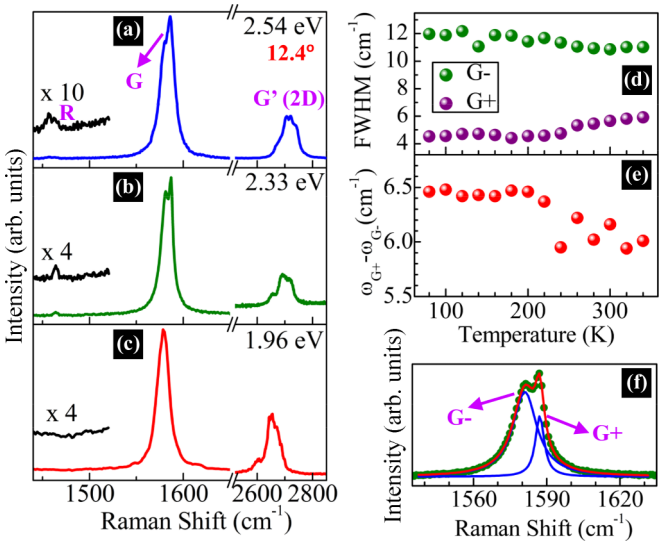

FIG. 5. (Color online) (a)–(c) Laser-excitation energy-dependent Raman spectra of folded tetralayer graphene of θ_{medium}. (d), (e) Peak width of the $G+$ mode and $G-$ mode and the frequency separation between the $G+$ mode and $G-$ mode as a function of temperature under the excitation energy of 2.33 eV for folded tetralayer graphene of θ_{medium}, respectively. (f) Raman spectrum of G mode with fitted curves shown in (b).

is resonantly enhanced, and simultaneously the weak R peak is also activated. It is noticed that the position of R peak here (1464 cm^{-1}) is smaller than that of the R peak in our θ_{medium} fDLG, meaning a larger rotational angle should be expected [29], which is clearly demonstrated by our measurements [Fig. 1(c) and Fig. 4(c)]. Furthermore, the same as the normal G mode, this new peak ($G+$) is also nondispersive, indicating it might be a zone center phonon too. The linewidths and the intensity ratios of two split G peaks could be sensitive indicators of the asymmetric doping levels, where phonon mixing may exist [49]. The detailed curve fitting [Fig. 5(f)] of the G mode in our θ_{medium} f4LG provides more spectral parameters of the split G peaks: The ratio of full width at half maximum (FWHM) between $G-$ peak and $G+$ peak is ~2.3, and the relative intensity ratio of $G+$ peak to $G-$ peak (I_{G+}/I_{G-}) is around 0.3. Comparing these features together with the parameters of another θ_{medium} 2 + 2 f4LG (Supplemental Material Fig. S4 and Table S1 [36]) with the spectral parameters of the asymmetrically doped BLG, it is noticed that our case is very much different from the optical phonon mixing in asymmetrically doped BLG. For example, the linewidth ratios ($\text{FWHM}_{G-}/\text{FWHM}_{G+}$) of our two θ_{medium} 2 + 2 f4LG samples are around 2.3, but their I_{G+}/I_{G-} could be very different [1.25 in Supplemental Material Fig. S4 [36] and 0.31 in Fig. 5(f)]. On a clear contrast, for such a ratio of $G-$ width over $G+$ width (~2.3), the I_{G+}/I_{G-} of two G peaks induced by the phonon mixing is always very small, near 0.1 [49,51]. The line shapes of the Raman G band are also very different between our θ_{medium} 2 + 2 f4LG and the one caused by the phonon mixing in the asymmetrically doped BLG. For example, for phonon mixing, when the peak widths are quite different, one of the split peaks is so dominant that the overall spectra appear as one broad peak [49,51], while one narrow and one broad peak are obviously present in the spectra of our samples. The different relative intensities among our folded graphene samples might be dependent on the twisting angles and, consequently, the evolution of the band structures for a given excitation energy, which will be further studied through our ongoing projects.

The observation of the narrow $G+$ mode rules out the possibility that this $G+$ peak is due to strain, as the $G+$ peak appears as broad as the $G-$ peak for the strain case [15,16]. Considering the above findings and discussions, we speculate that the $G+$ mode in the θ_{medium} f4LG is an IR-active mode E_{1u}, which might be activated and enhanced by the stacking defect, the twist of a unique twisting angle, i.e. θ_{medium}, in this paper. Our temperature-dependent Raman measurements strongly support this speculation. The temperature-dependent Raman spectra in the G mode region with fitted curves of θ_{medium} f4LG are shown in Supplemental Material Fig. S5 [36]. Figures 5(d) and (e) present the FWHM and the peak position separation of the $G-$ (E_{2g}) mode and the $G+$ (E_{1u}) mode, respectively, as a function of temperatures. As can be clearly seen, with the decrease of the temperatures, the linewidth of the $G+$ mode decreases while the $G-$ mode becomes slightly broader. The vibrational energy separation of these two modes increases as a consequence of a bit faster hardening of the $G+$ mode as compared to the $G-$ mode with a decrease of temperatures. This shows a good agreement with previous studies and could be explained by the different electron-phonon anharmonic scattering in the Raman- and IR-active modes for the linewidths and the presence (absence) of the coupling between E_{1u} (E_{2g}) phonon and a low wave number out-of-plane optical phonon for the separation of peak positions [53]. Even though in this paper we demonstrate that the enhancement of G mode and the splitting of G' mode in a 1 + 1 fDLG of rotational angle of 10.8° and the splitting of G mode in a 2 + 2 f4LG of rotational angle of 12.4°, it is worth noting that the rotational angles, θ_{medium}, which initiate the enhancement of the G mode and the doublet splitting of G' and G modes in folded graphene layers, are dependent on the excitation photon energies and may vary by a few degrees under different excitation energies.

IV. CONCLUSIONS

In summary, we have systematically investigated the Raman G and G' modes of 1 + 1 and 2 + 2 folded graphene layers. Three types of folded samples corresponding to three ranges (small, medium, and large) of rotational angles are classified by evaluating and comparing their Raman spectral features to those of pristine SLG and Bernal-stacked BLG. The evolution of the Raman G and G' modes in fDLG and f4LG under different excitation energies are studied. A doublet splitting of the G' mode in the θ_{medium} fDLG and the G mode in the θ_{medium} f4LG is observed and well explained by the coexistence of (i) the inner and the outer scattering modes and the trigonal warping effects, as well as further downward bending of the inner dispersion branch at visible excitation energy, and (ii) the Raman-active and the stacking defect activated IR-active mode, respectively, through the systematic investigations of the polarization and temperature-dependent Raman spectroscopy. This paper provides (i) the overall picture of the Raman spectra of the folded graphene layers,

(ii) the evolution of the dominant Raman modes, and (iii) an understanding of the doublet splitting of the G and G' modes in the θ_{medium} folded graphene layers. It successfully demonstrates that Raman imaging/spectroscopy is indeed a unique and powerful tool for probing the electron-phonon coupling and electronic band structures for both Bernal- and non-Bernal-stacked graphene layers.

ACKNOWLEDGMENTS

This paper is supported by the Singapore National Research Foundation under NRF RF Award No. NRF-RF2010-07 and Ministry of Education (MOE) Tier 2 MOE2012-T2-2-049. The authors are grateful for the valuable help of Dr. Jeil Jung for the density of states simulation.

[1] A. C. Ferrari and D. M. Basko, Nat. Nanotechnol. **8**, 235 (2013).
[2] A. C. Ferrari, J. C. Meyer, V. Scardaci, C. Casiraghi, M. Lazzeri, F. Mauri, S. Piscanec, D. Jiang, K. S. Novoselov, S. Roth, and A. K. Geim, Phys. Rev. Lett. **97**, 187401 (2006).
[3] L. M. Malard, J. Nilsson, D. L. Mafra, D. C. Elias, J. C. Brant, F. Plentz, E. S. Alves, A. H. C. Neto, and M. A. Pimenta, Phys. Status Solidi B **245**, 2060 (2008).
[4] M. S. Dresselhaus, A. Jorio, and R. Saito, Annu. Rev. Condens. Matter Phys. **1**, 89 (2010).
[5] L. M. Malard, M. A. Pimenta, G. Dresselhaus, and M. S. Dresselhaus, Phys. Rep. **473**, 51 (2009).
[6] A. Gupta, G. Chen, P. Joshi, S. Tadigadapa, and P. C. Eklund, Nano Lett. **6**, 2667 (2006).
[7] X. C. Dong, Y. M. Shi, Y. Zhao, D. M. Chen, J. Ye, Y. G. Yao, F. Gao, Z. H. Ni, T. Yu, Z. X. Shen, Y. X. Huang, P. Chen, and L. J. Li, Phys. Rev. Lett. **102**, 135501 (2009).
[8] X. C. Dong, D. L. Fu, W. J. Fang, Y. M. Shi, P. Chen, and L. J. Li, Small **5**, 1422 (2009).
[9] N. Peimyoo, T. Yu, J. Z. Shang, C. X. Cong, and H. P. Yang, Carbon **50**, 201 (2012).
[10] J. Yan, Y. B. Zhang, P. Kim, and A. Pinczuk, Phys. Rev. Lett. **98**, 166802 (2007).
[11] J. Yan, E. A. Henriksen, P. Kim, and A. Pinczuk, Phys. Rev. Lett. **101**, 136804 (2008).
[12] A. Das, S. Pisana, B. Chakraborty, S. Piscanec, S. K. Saha, U. V. Waghmare, K. S. Novoselov, H. R. Krishnamurthy, A. K. Geim, A. C. Ferrari, and A. K. Sood, Nat. Nanotechnol. **3**, 210 (2008).
[13] S. Pisana, M. Lazzeri, C. Casiraghi, K. S. Novoselov, A. K. Geim, A. C. Ferrari, and F. Mauri, Nat. Mater. **6**, 198 (2007).
[14] T. Yu, Z. H. Ni, C. L. Du, Y. M. You, Y. Y. Wang, and Z. X. Shen, J. Phys. Chem. C **112**, 12602 (2008).
[15] T. M. G. Mohiuddin, A. Lombardo, R. R. Nair, A. Bonetti, G. Savini, R. Jalil, N. Bonini, D. M. Basko, C. Galiotis, N. Marzari, K. S. Novoselov, A. K. Geim, and A. C. Ferrari, Phys. Rev. B **79**, 205433 (2009).
[16] M. Y. Huang, H. G. Yan, C. Y. Chen, D. H. Song, T. F. Heinz, and J. Hone, Proc. Natl. Acad. Sci. USA **106**, 7304 (2009).
[17] Z. H. Ni, T. Yu, Y. H. Lu, Y. Y. Wang, Y. P. Feng, and Z. X. Shen, ACS Nano **2**, 2301 (2008).
[18] S. Reich and C. Thomsen, Philos. Trans. R. Soc. A **362**, 2271 (2004).
[19] A. G. Souza Filho, A. Jorio, A. K. Swan, M. S. Ünlü, B. B. Goldberg, R. Saito, J. H. Hafner, C. M. Lieber, M. A. Pimenta, G. Dresselhaus, and M. S. Dresselhaus, Phys. Rev. B **65**, 085417 (2002).
[20] C. H. Lui, Z. Q. Li, Z. Y. Chen, P. V. Klimov, L. E. Brus, and T. F. Heinz, Nano Lett. **11**, 164 (2011).
[21] C. X. Cong, T. Yu, K. Sato, J. Z. Shang, R. Saito, G. F. Dresselhaus, and M. S. Dresselhaus, ACS Nano **5**, 8760 (2011).
[22] J. M. B. Lopes dos Santos, N. M. R. Peres, and A. H. Castro Neto, Phys. Rev. Lett. **99**, 256802 (2007).
[23] Z. H. Ni, Y. Y. Wang, T. Yu, Y. M. You, and Z. X. Shen, Phys. Rev. B **77**, 235403 (2008).
[24] Z. H. Ni, L. Liu, Y. Y. Wang, Z. Zheng, L. J. Li, T. Yu, and Z. X. Shen, Phys. Rev. B **80**, 125404 (2009).
[25] A. K. Gupta, Y. J. Tang, V. H. Crespi, and P. C. Eklund, Phys. Rev. B **82**, 241406 (2010).
[26] V. Carozo, C. M. Almeida, E. H. M. Ferreira, L. G. Cancado, C. A. Achete, and A. Jorio, Nano Lett. **11**, 4527 (2011).
[27] V. Carozo, C. M. Almeida, B. Fragneaud, P. M. Bedê, M. V. O. Moutinho, J. Ribeiro-Soares, N. F. Andrade, A. G. Souza Filho, M. J. S. Matos, B. Wang, M. Terrones, R. B. Capaz, A. Jorio, C. A. Achete, and L. G. Cançado, Phys. Rev. B **88**, 085401 (2013).
[28] R. W. Havener, H. L. Zhuang, L. Brown, R. G. Hennig, and J. Park, Nano Lett. **12**, 3162 (2012).
[29] J. Campos-Delgado, L. G. Cancado, C. A. Achete, A. Jorio, and J. P. Raskin, Nano Res **6**, 269 (2013).
[30] K. Kim, S. Coh, L. Z. Tan, W. Regan, J. M. Yuk, E. Chatterjee, M. F. Crommie, M. L. Cohen, S. G. Louie, and A. Zettl, Phys. Rev. Lett. **108**, 246103 (2012).
[31] G. H. Li, A. Luican, J. M. B. L. dos Santos, A. H. C. Neto, A. Reina, J. Kong, and E. Y. Andrei, Nat. Phys. **6**, 109 (2010).
[32] R. He, T. F. Chung, C. Delaney, C. Keiser, L. A. Jauregui, P. M. Shand, C. C. Chancey, Y. N. Wang, J. M. Bao, and Y. P. Chen, Nano Lett. **13**, 3594 (2013).
[33] C. C. Lu, Y. C. Lin, Z. Liu, C. H. Yeh, K. Suenaga, and P. W. Chiu, ACS Nano **7**, 2587 (2013).
[34] Z. H. Ni, H. M. Wang, J. Kasim, H. M. Fan, T. Yu, Y. H. Wu, Y. P. Feng, and Z. X. Shen, Nano Lett. **7**, 2758 (2007).
[35] S. Coh, L. Z. Tan, S. G. Louie, and M. L. Cohen, Phys. Rev. B **88**, 165431 (2013).
[36] See Supplemental Material at http://link.aps.org/supplemental/10.1103/PhysRevB.89.235430 for the following items: rotational angles determination, G' mode evolution of $1+1$ θ_{small} folded double-layer graphene together with that of AB-stacked BLG under different excitation photon energies, schematic diagram of outer and inner scattering processes of G' band in $1+1$ fDLG of θ_{medium}, doublet splitting of G mode in another $2+2$ f4LG samples of θ_{medium}, *in situ* temperature-dependent Raman spectra of $2+2$ θ_{medium} folded tetra-layer graphene, doublet splitting of G' mode in another $1+1$ folded double-layer graphene samples of θ_{medium}, and twisting angle distribution of more than 20 different folded $1+1$ and $2+2$ samples followed into three ranges of rotational angles according to the three patterns of Raman G and G' modes discussed in this paper.

[37] Y. M. You, Z. H. Ni, T. Yu, and Z. X. Shen, Appl. Phys. Lett. **93**, 163112 (2008).
[38] C. X. Cong, T. Yu, and H. M. Wang, ACS Nano **4**, 3175 (2010).
[39] L. G. Cancado, M. A. Pimenta, B. R. A. Neves, M. S. S. Dantas, and A. Jorio, Phys. Rev. Lett. **93**, 247401 (2004).
[40] E. SuarezMorell, J. D. Correa, P. Vargas, M. Pacheco, and Z. Barticevic, Phys. Rev. B **82**, 121407 (2010).
[41] Z. Q. Luo, C. X. Cong, J. Zhang, Q. H. Xiong, and T. Yu, Appl. Phys. Lett. **100**, 243107 (2012).
[42] S. Berciaud, X. L. Li, H. Htoon, L. E. Brus, S. K. Doorn, and T. F. Heinz, Nano Lett. **13**, 3517 (2013).
[43] D. Yoon, Y. W. Son, and H. Cheong, Phys. Rev. Lett. **106**, 155502 (2011).
[44] O. Frank, M. Mohr, J. Maultzsch, C. Thomsen, I. Riaz, R. Jalil, K. S. Novoselov, G. Tsoukleri, J. Parthenios, K. Papagelis, L. Kavan, and C. Galiotis, ACS Nano **5**, 2231 (2011).
[45] R. Narula, N. Bonini, N. Marzari, and S. Reich, Phys. Rev. B **85**, 115451 (2012).
[46] P. Venezuela, M. Lazzeri, and F. Mauri, Phys. Rev. B **84**, 035433 (2011).
[47] A. Grüneis, R. Saito, Ge. G. Samsonidze, T. Kimura, M. A. Pimenta, A. Jorio, A. G. Souza Filho, G. Dresselhaus, and M. S. Dresselhaus, Phys. Rev. B **67**, 165402 (2003).
[48] C. X. Cong and T. Yu, arXiv:1312.6928 (2013).
[49] W. J. Zhao, P. H. Tan, J. Zhang, and J. A. Liu, Phys. Rev. B **82**, 245423 (2010).
[50] T. Ando and M. Koshino, J. Phys. Soc. Jpn. **78**, 034709 (2009).
[51] J. Yan, T. Villarson, E. A. Henriksen, P. Kim, and A. Pinczuk, Phys. Rev. B **80**, 241417 (2009).
[52] P. Gava, M. Lazzeri, A. M. Saitta, and F. Mauri, Phys. Rev. B **80**, 155422 (2009).
[53] P. Giura, N. Bonini, G. Creff, J. B. Brubach, P. Roy, and M. Lazzeri, Phys. Rev. B **86**, 121404 (2012).